

Experimental study of turbulent thermal diffusion of inertial particles in a convective turbulence forced by oscillating grids

E. Elmakies, O. Shildkrot, N. Kleeorin, A. Levy, and I. Rogachevskii*

The Pearlstone Center for Aeronautical Engineering Studies, Department of Mechanical Engineering, Ben-Gurion University of the Negev, P.O.Box 653, Beer-Sheva 8410530, Israel

(Dated: February 26, 2026)

We investigate the phenomenon of turbulent thermal diffusion of inertial solid particles in laboratory experiments with convective turbulence forced by one or two oscillating grids in the air flow. Turbulent thermal diffusion causes a non-diffusive contribution to turbulent flux of particles described in terms of an effective pumping velocity directed opposite to the gradient of the mean fluid temperature. For inertial particles, this effective pumping velocity depends on the Stokes and Reynolds numbers. In the experiments, fluid velocity and spatial distribution of inertial particles are measured using Particle Image Velocimetry system, and the temperature field is measured in many locations by a temperature probe equipped with 12 thermocouples. Measurements of temperature and particle number density spatial distributions have demonstrated formation of large-scale clusters of inertial particles in the vicinity of the mean temperature minimum due to turbulent thermal diffusion. In the experiments, the effective pumping velocity resulting in formation of large-scale clusters of inertial particles (having the diameter $10\mu\text{m}$) is in 2.5 times larger than that for non-inertial particles (having the diameter $0.7\mu\text{m}$). This is in an agreement with the theoretical predictions.

I. INTRODUCTION

Turbulent transport of particles has been investigated more than hundred years due to a number of applications in astrophysical, geophysical and industrial flows [1–7]. However, some key questions are still a subject of various discussions.

There are various phenomena associated with formation of large-scale particle clusters in small-scale turbulence. The spatial scales of the particle clusters are much larger than the integral turbulence scale and their lifetimes are much longer than the turbulent time. Key phenomena creating large-scale particle clusters are turbophoresis of inertial particles in an isothermal inhomogeneous turbulence [8, 9] and turbulent thermal diffusion in a temperature-stratified turbulence [10, 11].

Turbophoresis is interpreted in terms of an effective pumping velocity $\bar{\mathbf{V}}_{\text{turb}} \propto -\kappa_{\text{turb}} \nabla \langle \mathbf{u}^2 \rangle$ of inertial particles, where \mathbf{u} are velocity fluctuations and κ_{turb} is the turbophoretic coefficient which depends on the Stokes and Reynolds numbers [8, 9, 12–19]. Turbophoresis results in formation of large-scale particle clusters in the regions with the minimum turbulence intensity.

Turbulent thermal diffusion is described by the effective pumping velocity $\mathbf{V}^{\text{eff}} = -\alpha D_{\text{T}} \nabla \ln \bar{T}$ in a temperature-stratified turbulence, where the turbulent flux of particles $\langle n' \mathbf{u} \rangle = \mathbf{V}^{\text{eff}} \bar{n} - D_{\text{T}} \nabla \bar{n}$. Here \bar{n} is the mean particle number density, \bar{T} is the mean temperature of the fluid, D_{T} is the turbulent diffusion coefficient and n' are fluctuations of particle number density. For non-inertial particles the parameter $\alpha = 1$, while for inertial

particles the parameter α is given by [7, 10, 11, 13]

$$\alpha = 1 + 2 \frac{V_{\text{g}} L_P \ln \text{Re}}{u_0 \ell_0}, \quad (1)$$

where $\mathbf{V}_{\text{g}} = \tau_{\text{p}} \mathbf{g}$ is the terminal fall velocity of inertial particles, $\tau_{\text{p}} = m_{\text{p}} / (3\pi\rho\nu d_{\text{p}})$ is the Stokes time, \mathbf{g} is the acceleration due to the gravity, ρ is the fluid density, ν is the kinematic viscosity, m_{p} and d_{p} are the particle mass and diameter, respectively, $L_P = |\nabla_z \bar{P} / \bar{P}|^{-1}$ is the pressure height scale, \bar{P} is the mean pressure, $\text{Re} = u_0 \ell_0 / \nu$ is the Reynolds number, and u_0 is the characteristic turbulent velocity in the integral scale ℓ_0 .

The mean particle number density of inertial particles is determined by the following equation:

$$\frac{\partial \bar{n}}{\partial t} + \nabla \cdot \left[\left(\bar{\mathbf{U}} + \mathbf{V}_{\text{g}} - \alpha D_{\text{T}} \frac{\nabla \bar{T}}{\bar{T}} \right) \bar{n} - D_{\text{T}} \nabla \bar{n} \right] = 0, \quad (2)$$

where $\bar{\mathbf{U}}$ is the mean fluid velocity. Here we neglect small molecular (Brownian) diffusion coefficient D for large Péclet numbers. Equation (2) is obtained by averaging of equation for the particle number density over an ensemble of turbulent velocity field.

For simplicity, we assume that the gradients along the vertical axis Z of the mean temperature, mean velocity, mean number density and turbulent diffusion coefficient are much larger than those in other directions. This condition corresponds to that observed in the experiments discussed in this paper. The steady-state solution for Eq. (2) for a zero total particle flux at the boundaries reads

$$\frac{\bar{n}(Z)}{\bar{n}_{\text{b}}} = \left(\frac{\bar{T}(Z)}{\bar{T}_{\text{b}}} \right)^{-\alpha} \exp \left(\int_0^Z \frac{\bar{U}_z - V_{\text{g}}}{D_z^{\text{T}}} dZ' \right), \quad (3)$$

* gary@bgu.ac.il

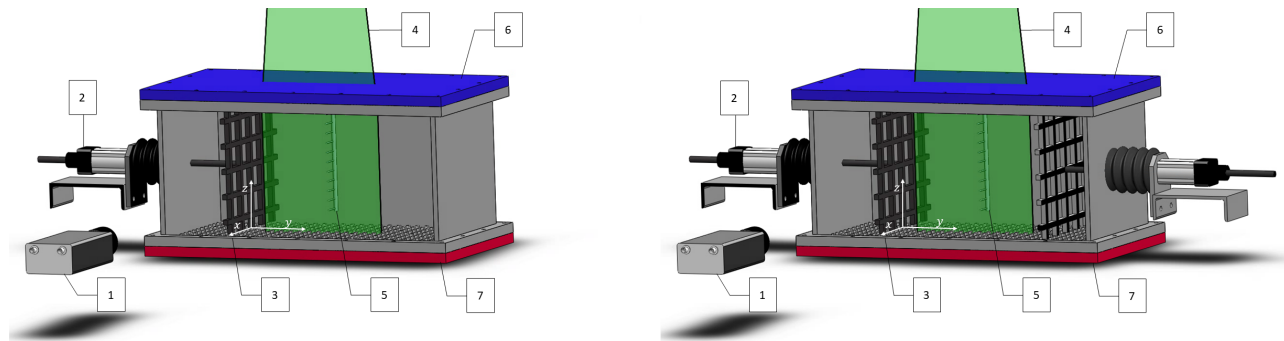


FIG. 1. Experimental setup with the convective turbulence forced by one oscillating grid (left panel) and by two oscillating grids (right panel): (1) digital CCD camera; (2) rod driven by the speed-controlled motor; (3) oscillating grid; (4) laser light sheet; (5) temperature probe equipped with 12 E - thermocouples; (6) heat exchanger at the top cooled wall of the chamber; (7) heat exchanger at the bottom heated wall of the chamber.

where $D_z^T = \ell_z [\langle u_z^2 \rangle]^{1/2}$ is the vertical turbulent diffusion coefficient, and the boundary conditions are $\bar{n}_b = \bar{n}(Z = 0)$ and $\bar{T}_b = \bar{T}(Z = 0)$. Equation (3) implies that maximum particle number density is attained near the region with minimum mean fluid temperature. Therefore, turbulent thermal diffusion causes formation of large-scale particle clusters in the vicinity of the mean temperature minimum.

Turbulent thermal diffusion has been investigated analytically adopting various theoretical approaches (namely, the dimensional analysis, the quasi-linear approach, the τ approaches applied in physical and Fourier spaces, the path integral approach and the direct interaction approximation, see, e.g., Refs. [7, 10, 11, 13, 20–25]). This phenomenon has been found in direct numerical simulations [26, 27]. This effect has been studied in geophysical [28], planetary [29] and astrophysical [30, 31] turbulence applications.

Phenomenon of turbulent thermal diffusion has been detected in laboratory experiments in the air flow with micron-size particles in temperature stratified turbulence produced by one or two oscillating grids [25, 32–36], by multi-fan turbulence generator [37] and in strongly inhomogeneous and anisotropic convection forced by two similar turbulence generators with oscillating membrane and a steady grid in the air flow [38]. This phenomenon has been even found for nanoparticles [39] in turbulent convection. However, turbulent thermal diffusion has not been yet comprehensively investigated for inertial particles in laboratory experiments.

In the present study, we investigate phenomenon of turbulent thermal diffusion of inertial solid particles in experiments with a convective turbulence forced by one or two oscillating grids in the air flow. This paper is organized as follows. In Sec. II we describe experimental setup and measurement techniques. In Sec. III we analyse the obtained experimental results, and in Sec. IV we outline conclusions.

II. EXPERIMENTAL SETUP

In this section we describe the experimental set-up and measurement technique. We study phenomenon of turbulent thermal diffusion of inertial solid particles in experiments with a convective turbulence forced by one or two oscillating grids in the air flow. We conduct experiments in rectangular transparent chamber with dimensions $L_x \times L_y \times L_z$ with $L_x = L_z = 26$ cm and $L_y = 53$ cm, where Z is directed along the vertical direction and Y is perpendicular to the grid plain. The oscillating grids with bars arranged in a square array are parallel to the side walls of the chamber, and are positioned at a distance of two grid meshes from the side walls of the chamber (see Fig. 1).

Two aluminium heat exchangers with rectangular pins $3 \times 3 \times 15$ mm are attached to the bottom (heated) and top (cooled) walls of the chamber, which allow one to form a large vertical mean temperature gradient in the core of the fluid flow. The temperature field is measured in many locations by means of a temperature probe equipped with 12 E - thermocouples. The thermocouples with the diameter of 0.13 mm and the sensitivity of $\approx 75 \mu\text{V/K}$ are attached to a vertical rod with a diameter 4 mm, and the mean distance between thermocouples is about 21.6 mm (see for details Ref. [35]). The data are recorded using the developed software based on LabView 2024 Q1, and the temperature maps are obtained using Matlab R2024a.

The velocity field is measured with a Particle Image Velocimetry (PIV) system [40–42], consisting in a Nd-YAG laser (Continuum Surelite 2×170 mJ) and a progressive-scan 12 bit digital CCD camera (with pixel size $6.45 \mu\text{m} \times 6.45 \mu\text{m}$ and 1376×1040 pixels). As a tracer for the PIV measurements, we use an incense smoke with spherical solid particles having the mean diameter of $0.7 \mu\text{m}$ and the material density $\rho_p \approx 10^3 \bar{\rho}$, where $\bar{\rho}$ is the mean fluid density. The particles are produced by high temperature sublimation of solid incense grains (see for details Ref. [35]).

The velocity fields in the experiments have been mea-

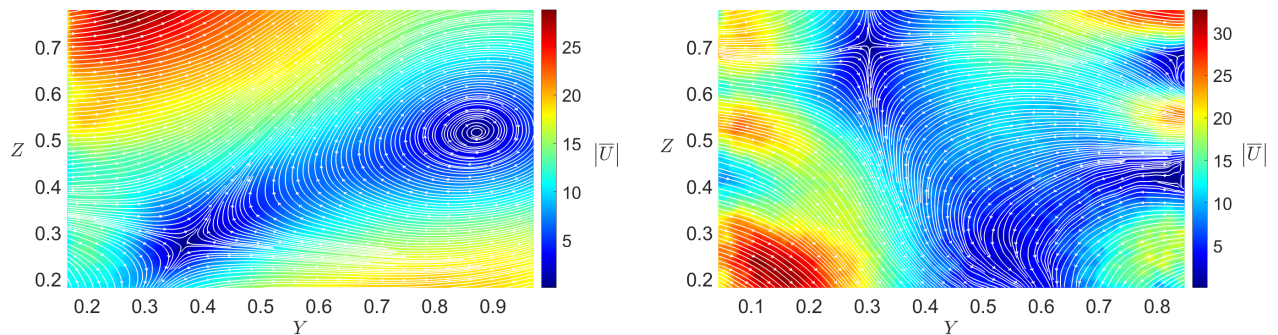


FIG. 2. Distributions of the mean velocity field \bar{U} for convective turbulence forced by one oscillating grid (left panel) and by two oscillating grids (right panel). The coordinates Y and Z are normalized by $L_z = 26$ cm. The mean velocity \bar{U} is measured in cm/s.

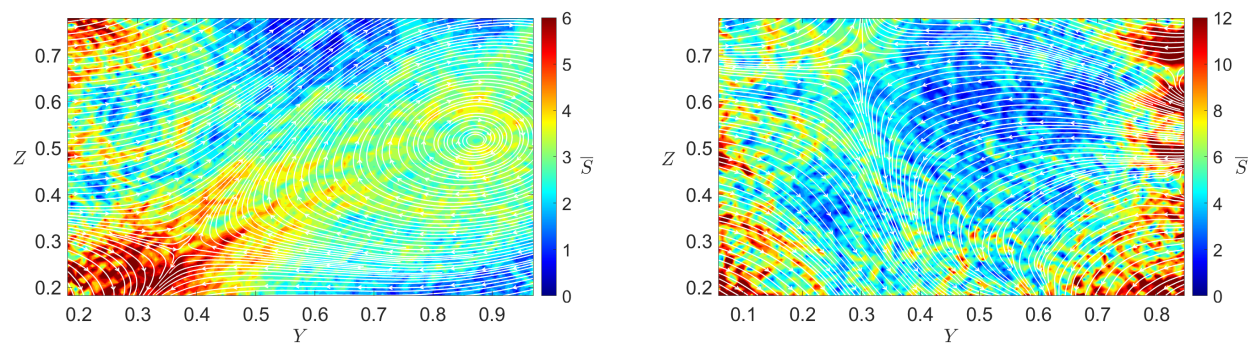


FIG. 3. Distributions of the mean velocity shear $\bar{S} = [(\nabla_y \bar{U}_y)^2 + (\nabla_z \bar{U}_y)^2 + (\nabla_y \bar{U}_z)^2 + (\nabla_z \bar{U}_z)^2]^{1/2}$ for convective turbulence forced by one oscillating grid (left panel) and by two oscillating grids (right panel). The streamlines (white) of the mean velocity \bar{U} are also superimposed on this distribution. The coordinates Y and Z are normalized by $L_z = 26$ cm, The mean velocity shear \bar{S} is measured in s^{-1} .

sured in a flow domain 209.1×155.4 mm² with a spatial resolution of 1376×1024 pixels, so that a spatial resolution $151 \mu\text{m}$ /pixel have been achieved. We analyse the velocity field in the probed region with interrogation windows of 16×16 pixels. Using the velocity measurements, various mean-field (see Figs. 2–3) and turbulent (see Figs. 4–11) characteristics have been obtained in our experiments. In particular, we determine the mean velocity field and mean velocity shear, the root mean square (r.m.s.) velocities, the turbulent anisotropy parameter, the two-point correlation functions of velocity field and the integral scales of turbulence. In particular, the integral length scales of turbulence ℓ_y and ℓ_z are calculated in the horizontal Y and the vertical Z directions from the two-point correlation functions of the velocity field. The mean and r.m.s. velocities are determined for every point of a velocity map by averaging over 530 independent maps. In the experiments we evaluated the variability between the first and the last 20 velocity maps of the series of the measured velocity field. Since very small variability is found, these tests show that 520 velocity maps contain enough data to obtain reliable statistical estimates. The size of the probed region does not affect

our results.

In our experiments, the spatial distributions for particles having the diameters $0.7 \mu\text{m}$ and $10 \mu\text{m}$ are obtained by the PIV system using the effect of the Mie light scattering by particles [43]. In particular, the mean intensity of scattered light is determined in 85×64 interrogation windows with the size 32×32 pixels (in convective turbulence forced by one oscillating grid), and in 65×51 interrogation windows with the size 32×32 pixels (in convective turbulence forced by two oscillating grids), with 50 % overlap (for better averaging data and smoothness). This allows us to find the vertical distribution of the intensity of the scattered light in 80 vertical strips composed of 64 interrogation windows. Here we take into account that the light radiation energy flux scattered by small particles is given by $E_s \propto E_0 \Psi(\pi d_p / \lambda; a_0; n)$, where Ψ is the scattering function, d_p is the particle diameter, λ is the wavelength, and a_0 is the index of refraction. The energy flux incident at the particle is given by $E_0 \propto \pi d_p^2 / 4$. For $\lambda > \pi d_p$, the scattering function Ψ is determined by the Rayleigh's law, $\Psi \propto d_p^4$. For $\lambda < \pi d_p$, the scattering function Ψ is independent of the particle diameter and the wavelength. In a general case, the scattering function

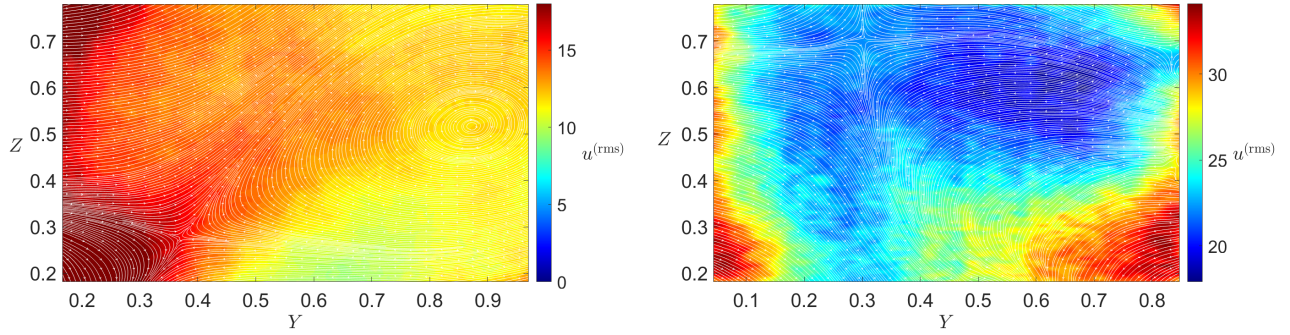


FIG. 4. Distributions of the turbulent velocity $|u^{(\text{rms})}| = [\langle u_y^2 \rangle + \langle u_z^2 \rangle]^{1/2}$ for convective turbulence forced by one oscillating grid (left panel) and by two oscillating grids (right panel). The streamlines (white) of the mean velocity \bar{U} are also superimposed on this distribution. The coordinates Y and Z are normalized by $L_z = 26$ cm.

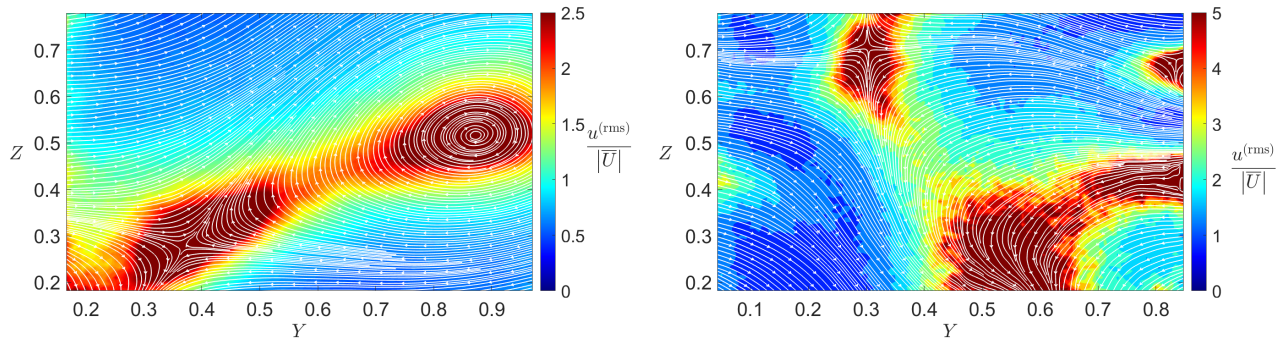


FIG. 5. Distributions of the ratio $u^{(\text{rms})}/|\bar{U}|$ for convective turbulence forced by one oscillating grid (left panel) and by two oscillating grids (right panel). The streamlines (white) of the mean velocity \bar{U} are also superimposed on this distribution. The coordinates Y and Z are normalized by $L_z = 26$ cm.

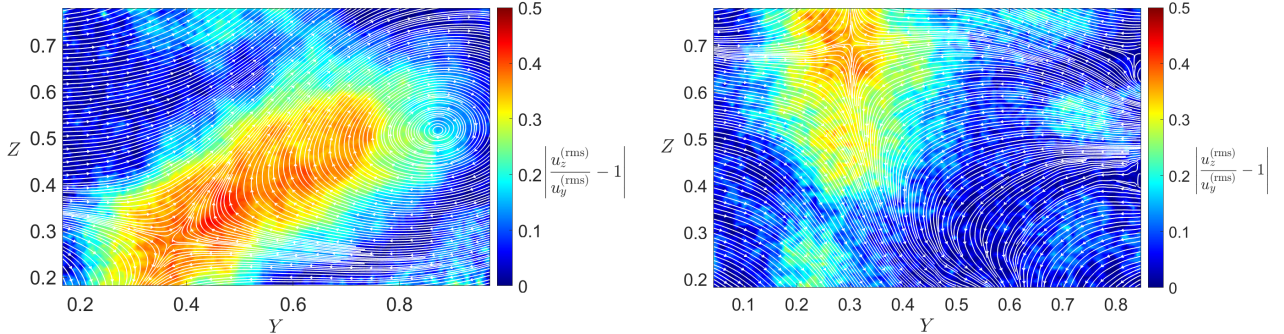


FIG. 6. Distributions of the anisotropy of turbulent velocity field $|u_z^{(\text{rms})}/u_y^{(\text{rms})} - 1|$ for convective turbulence forced by one oscillating grid (left panel) and by two oscillating grids (right panel). The streamlines (white) of the mean velocity \bar{U} are also superimposed on this distribution. The coordinates Y and Z are normalized by $L_z = 26$ cm.

Ψ is determined by the Mie equations [44]. The light radiation energy flux scattered by small particles is given by $E_s \propto E_0 n (\pi d_p^2/4)$, so that the scattered light energy flux incident on the charge-coupled device (CCD) camera probe is proportional to the particle number density n .

The scattered radiation intensity recorded by the CCD camera at a given spatial location is proportional to the

local particle number density. Therefore, intensity ratios obtained at that location in different measurements directly represent the corresponding ratios of particle number densities. For the normalization of the scattered light intensity E^T obtained in a temperature-stratified turbulence, the distribution of the scattered light intensity E measured in the isothermal case is used under the same

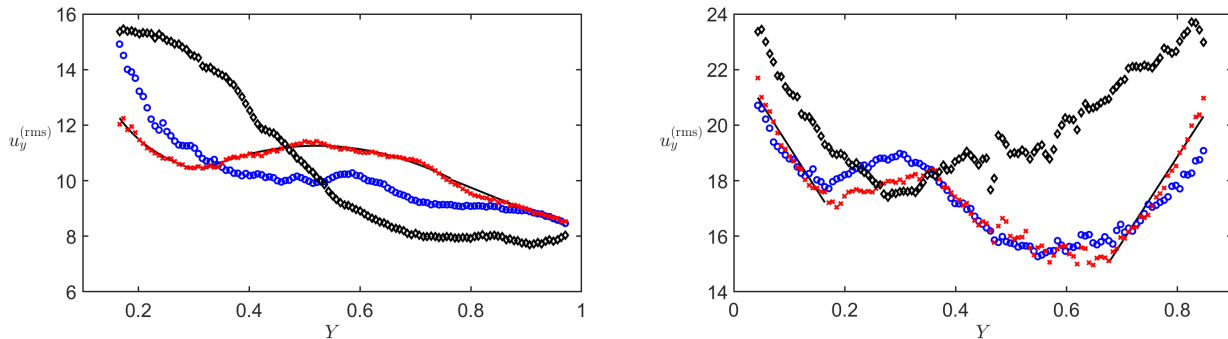


FIG. 7. Dependencies of the turbulent velocity $u_y^{(\text{rms})}(Y)$ on the horizontal coordinate Y in the core flow averaged over various ranges Z for convective turbulence forced by one oscillating grid (left panel) and by two oscillating grids (right panel). Fitting curves are shown by the solid lines. The averaging is over $Z = 4.7\text{-}9.2$ cm (blue, circles); $9.2\text{-}14.7$ cm (red, crosses); $14.7\text{-}20.3$ cm (black, diamonds). The velocity is measured in cm/s and the coordinates Y is normalized by $L_z = 26$ cm.

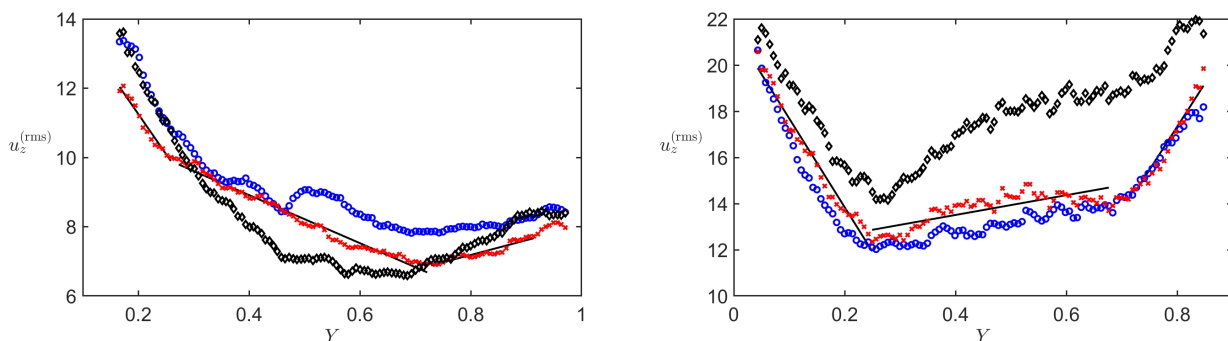


FIG. 8. Dependencies of the turbulent velocity $u_z^{(\text{rms})}(Y)$ on the horizontal coordinate Y in the core flow averaged over various ranges Z for convective turbulence forced by one oscillating grid (left panel) and by two oscillating grids (right panel). Fitting curves are shown by the solid lines. The left panel: the averaging is over $Z = 5.2\text{-}9.3$ cm (blue, circles); $9.2\text{-}14.3$ cm (red, crosses); $14.3\text{-}18.6$ cm (black, diamonds). The right panel: the averaging is over $Z = 5.3\text{-}9.4$ cm (blue, circles); $9.4\text{-}14.2$ cm (red, crosses); $14.2\text{-}18.4$ cm (black, diamonds). The velocity is measured in cm/s and the coordinates Y is normalized by $L_z = 26$ cm.

conditions. The distribution of the scattered light intensity averaged over a vertical coordinate is independent of the particle number density in the isothermal flow. Therefore, using this normalization, we can characterize the spatial distribution of particle number density $n \propto E^T/E$ in the non-isothermal turbulence.

For experimental study of turbulent thermal diffusion of inertial particles, we use borosilicate hollow glass particles having an approximately spherical shape, a mean diameter of $10\ \mu\text{m}$ and the material density $\rho_p \approx 1.4\ \text{g/cm}^3$. These particles have been injected in the chamber using an air jet to improve particle mixing and prevent from particle agglomeration.

We use a custom-made acoustic feeding device for injecting particles into the flow comprising an acrylic glass chamber with a size of $9 \times 9 \times 4\ \text{cm}^3$. Two plastic slabs inside the chamber are used as air guides to achieve optimal flow with entrained particles. Particle dispensation zone (a disk of 25 mm diameter and 5 mm thickness) is located at the bottom of the chamber. A standard woofer (oval $2 \times 3.5''$) at a frequency of 220 Hz sways a latex

membrane on which particles are loaded. A cylindrical cavity is used to contain the particles on the latex membrane. The batch of particles on the membrane should roughly fill the cavity. When the membrane vibrates, particles are entrained into air. Particle feeding device has a pressurized air inlet with bellows having a 8 mm diameter tube with standard quick release connector. The entrained particles leave the chamber with a stream of air through the outlet.

The measurement technique and data processing procedure described in this section are similar to those used by us in various experiments with turbulent convection [36, 39, 45–47] and stably stratified turbulence [35, 48, 49]. In addition, the similar measurement technique and data processing procedure in the experiments have been performed previously by us to investigate the phenomenon of turbulent thermal diffusion in a homogeneous turbulence [25, 32–34], mixing of particles in inhomogeneous turbulence [35, 36, 50], as well as for study of small-scale particle clustering [51].

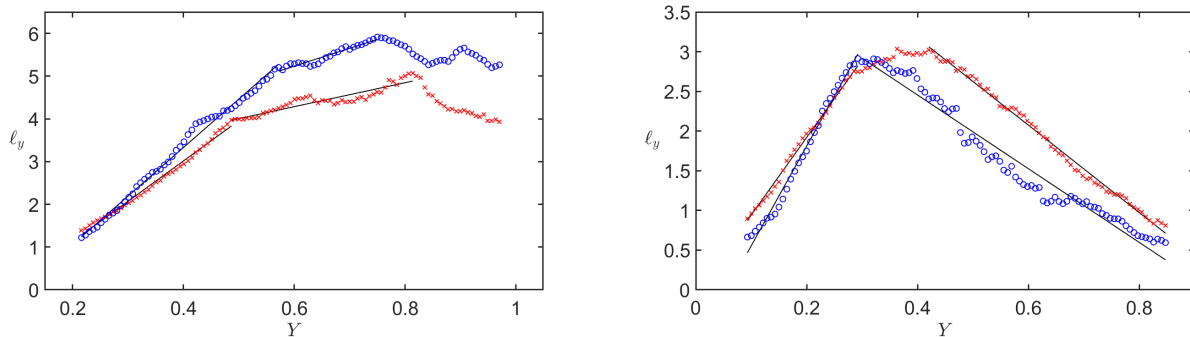


FIG. 9. Dependencies of the horizontal integral turbulence scale $\ell_y(Y)$ on the horizontal coordinate Y in the core flow averaged over Z for isothermal (red) and convective (blue) turbulence forced by one oscillating grid (left panel) and by two oscillating grids (right panel). Fitting curves are shown by the solid lines. The integral turbulence scale is measured in cm and the coordinates Y is normalized by $L_z = 26$ cm.

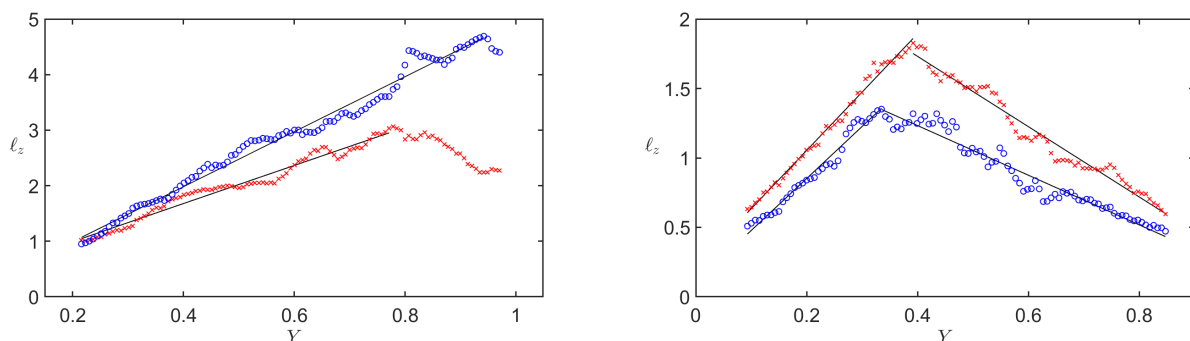


FIG. 10. Dependencies of the vertical integral turbulence scale $\ell_z(Y)$ on the horizontal coordinate Y in the core flow averaged over Z for isothermal (red) and convective (blue) turbulence forced by one oscillating grid (left panel) and by two oscillating grids (right panel). Fitting curves are shown by the solid lines. The integral turbulence scale is measured in cm and the coordinates Y is normalized by $L_z = 26$ cm.

III. EXPERIMENTAL RESULTS

In this section, we discuss the obtained experimental results on fluid turbulence, turbulent transport of inertial particles and formation of large-scale particle clusters in a convective turbulence forced by one or two oscillating grids in the air flow (see Fig. 1). In all experiments with turbulent convection, the temperature difference $\Delta T = 50$ K between the bottom and upper walls of the chamber is applied, and the frequency f of the grid oscillations is $f = 10.5$ Hz, which yields the maximum turbulence intensity in our experimental set-up.

In Fig. 2 we show the mean velocity field in the core flow for convective turbulence forced by one oscillating grid (left panel) and by two oscillating grids (right panel). The oscillating grids do not completely destroy the large-scale circulations, but their structures are strongly deformed. The mean velocity patterns in these experiments are very complicated containing one or two large-scale circulations. The large-scale velocity shear inside large-scale circulation is strong enough (see Fig. 3 where we show the distributions of the mean velocity shear

$\bar{S} = [(\nabla_y \bar{U}_y)^2 + (\nabla_z \bar{U}_y)^2 + (\nabla_y \bar{U}_z)^2 + (\nabla_z \bar{U}_z)^2]^{1/2}$ for convective turbulence).

Distributions of various turbulent characteristics in the core flow of the chamber have been obtained in the experiments with forced convective turbulence (see Figs. 4–11). In particular, in Fig. 4 we show the distributions of the turbulent velocity $|u^{(\text{rms})}| = [\langle u_y^2 \rangle + \langle u_z^2 \rangle]^{1/2}$. In these experiments, the turbulent kinetic energy is produced by buoyancy in convection and forcing produced by oscillating grids. Large-scale shear of the mean velocity fields also contributes to the turbulence production rate. This is clearly seen in Fig. 5, where we show the distributions of the ratio of turbulent to mean velocities $u^{(\text{rms})}/|\bar{U}|$ in convective turbulence forced by one oscillating grid (left panel) and by two oscillating grids (right panel). For visualization of various turbulent regions, the streamlines of the mean velocity field \bar{U} are also superimposed on this distribution. The turbulent velocity is larger inside the large-scale circulations and in the vicinity of various complicated large-scale flows (e.g., the stagnation points), where the large-scale shear is stronger.

For convective turbulence forced by two oscillating

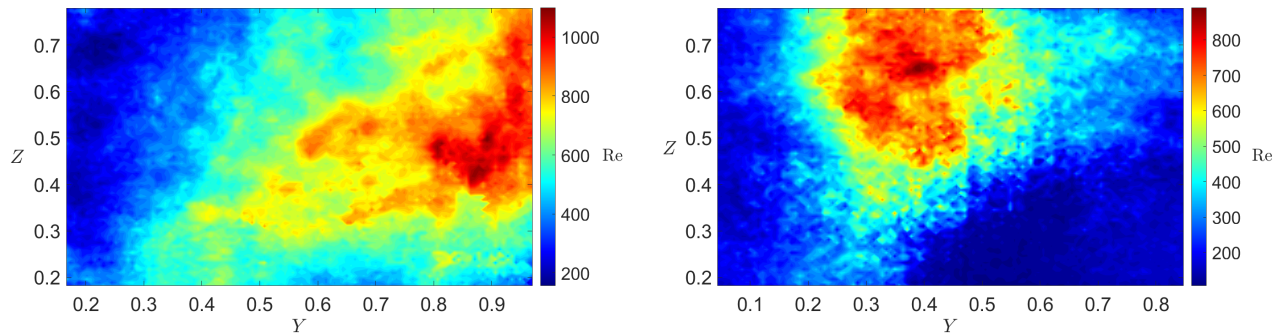


FIG. 11. Distributions of the Reynolds number $\text{Re} = (u_y^{(\text{rms})} \ell_y + 2u_z^{(\text{rms})} \ell_z) / \nu$ for convective turbulence forced by one oscillating grid (left panel) and by two oscillating grids (right panel). The coordinates Y and Z are normalized by $L_z = 26$ cm.

grids, the distributions of the turbulent velocity is more symmetric in core flow in the horizontal direction in comparison with that forced by one oscillating grid (see Figs. 4). The distributions of the turbulence anisotropy parameter $|u_z^{(\text{rms})} / u_y^{(\text{rms})} - 1|$ are shown in Fig. 6. The convective turbulence forced by two oscillating grids is less anisotropic in comparison with that forced by one oscillating grid.

In Figs. 7–10 we plot the dependencies of the horizontal and vertical turbulent velocities $u_y^{(\text{rms})}(Y)$ and $u_z^{(\text{rms})}(Y)$ and the horizontal and vertical integral turbulence scales $\ell_y(Y)$ and $\ell_z(Y)$ on the horizontal coordinate Y in the core flow. In various experiments with forced convection, we observe the scalings $\ell_i(Y) \propto Y$ in the left and right ranges of the horizontal coordinate Y . These scalings resemble qualitatively the results of the early laboratory experiments conducted with one oscillating grid in isothermal turbulence [52–58] and forced convective turbulence [35, 36, 38], where the integral turbulence length scale increases linearly with the distance Y from a grid.

The obtained components of the turbulent velocity and the integral turbulence scales allow us to estimate the Reynolds number based on turbulent characteristics, $\text{Re} = (u_y^{\text{rms}} \ell_y + 2u_z^{\text{rms}} \ell_z) / \nu$ (see Fig. 11). This expression for the Reynolds number estimate is obtained using the following arguments. The Reynolds number is estimated as $\text{Re} = \tau_0 \langle \mathbf{u}^2 \rangle / \nu$, where $\langle \mathbf{u}^2 \rangle = \langle u_x^2 \rangle + \langle u_y^2 \rangle + \langle u_z^2 \rangle$ and τ_0 is the turbulent time in the integral scale. We assume that the turbulent time is the same along X , Y and Z directions, i.e., $\tau_0 = \ell_x / u_x^{\text{rms}} = \ell_y / u_y^{\text{rms}} = \ell_z / u_z^{\text{rms}}$ and $u_x^{\text{rms}} \approx u_z^{\text{rms}}$. This yields the above estimate for the Reynolds number.

To investigate the phenomenon of turbulent thermal diffusion in a forced convective turbulence, we measure the spatial distributions of the mean temperature and the mean particle number density. The initial spatial distributions of particles injected into the chamber, are nearly homogeneous and isotropic. In a convective turbulence, the spatial distributions of the mean particle number density should be strongly inhomogeneous due to the effective pumping velocity $\mathbf{V}^{\text{eff}} = -\alpha D_T \nabla \ln \bar{T}$.

This results in accumulation of inertial particles in the vicinity of the mean temperature minimum.

In Fig. 12, we show the spatial distributions of the mean temperature $\bar{T}(Y, Z)$ in the core flow for turbulent convection forced by one oscillating grid (left panel) and by two oscillating grids (right panel). Maximum gradients of the mean temperature is observed in the vertical direction. In Fig. 13, we also show the spatial distributions of the normalised mean particle number density $\bar{n}(Y, Z) / \bar{n}_0$. The mean particle number density $\bar{n}(Y, Z)$ in every point in the experiments with forced convective turbulence is normalized by (i) the mean particle number density averaged over the vertical column, where all area in the horizontal direction is divided into 65 vertical columns; and (ii) the mean particle number density determined in the experiments with the isothermal turbulence.

In spite of the presence of the large-scale complicated fluid flows superimposed on the convective turbulence, Figs. 12–13 demonstrate the tendency of the localization of the maximum of the mean particle number density in the vicinity of the minimum in the mean temperature, and vice versa. In particular, particles are accumulated in the upper part of the chamber where the mean temperature field $\bar{T}(Y, Z)$ achieves the minimum values. As follows from Fig. 13, the maximum mean number density of inertial particles is observed in the right upper part of the chamber for turbulent convection forced by one oscillating grid, and in the left upper part of the chamber for turbulent convection forced by two oscillating grids.

This occurs by the following reasons. The Reynolds number reaches maximum values in the right part of the chamber for turbulent convection forced by one oscillating grid and in the left part of the chamber for turbulent convection forced by two oscillating grids (see Fig. 11). In these regions the turbulent diffusion coefficient D_T reaches the maximum values. Since the effective pumping velocity \mathbf{V}^{eff} of inertial particles is proportional to D_T , the velocity \mathbf{V}^{eff} also reaches the maximum values in these regions. This explains why in these regions the mean number density of inertial particles reaches maximum values. The above conclusions are valid in the tur-

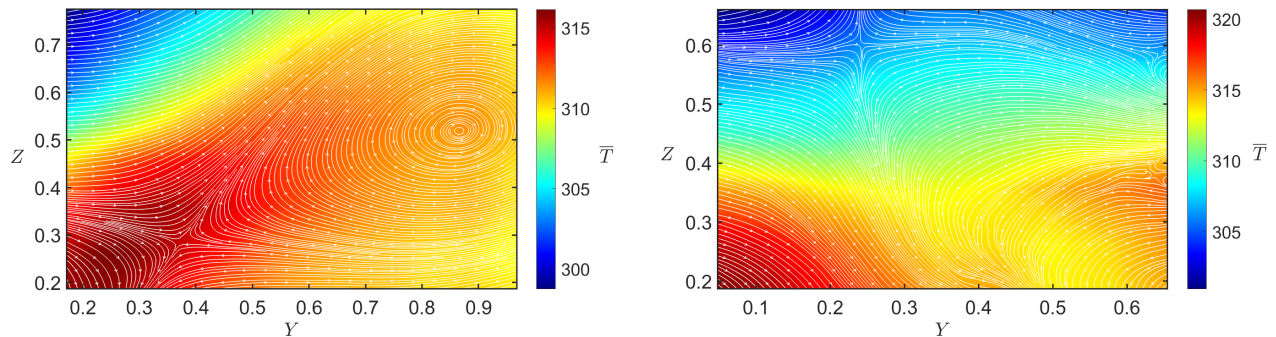


FIG. 12. Distributions of the mean temperature $\bar{T}(Y, Z)$ for convective turbulence forced by one oscillating grid (left panel) and by two oscillating grids (right panel). The streamlines (white) of the mean velocity \bar{U} are also superimposed on the temperature distribution. The coordinates Y and Z are normalized by $L_z = 26$ cm. The mean temperature $\bar{T}(Y, Z)$ is measured in K.

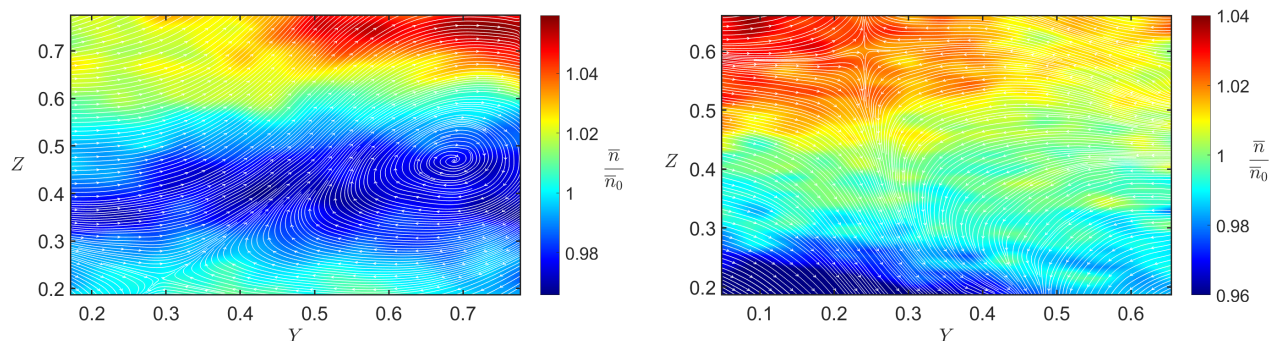


FIG. 13. Distributions of the normalized mean particle number density $\bar{n}(Y, Z)/\bar{n}_0$ for convective turbulence forced by one oscillating grid (left panel) and by two oscillating grids (right panel). The streamlines (white) of the mean velocity \bar{U} are also superimposed on the particle distribution. The coordinates Y and Z are normalized by $L_z = 26$ cm.

bulent regions with large mean temperature gradients. For these regions, the dominant effect of large-scale particle clustering is turbulent thermal diffusion. Deviations from this trend occurs in the regions with strong mean fluid motions where the mean temperature gradient is small.

For quantitative analysis of the experimental results, let us use the steady-state solution (3) for the equation for the mean particle number density \bar{n} . Taking into account that $\bar{T}(Z) = \bar{T}_b + \delta\bar{T}$, and expanding the function $(1 + \delta\bar{T}/\bar{T}_b)^{-\alpha} \approx 1 - \alpha(\delta\bar{T}/\bar{T}_b)$ in the Taylor series for $|\delta\bar{T}| \ll \bar{T}_b$, we obtain that

$$\frac{\bar{n}(Z)}{\bar{n}_b} \approx -\beta \frac{(\bar{T}(Z) - \bar{T}_b)}{\bar{T}_b}, \quad (4)$$

where $\bar{n}_b = \bar{n}(Z = 0)$ and $\bar{T}_b = \bar{T}(Z = 0)$, and the parameter β is

$$\beta = \alpha \exp\left(\int_0^Z \frac{\bar{U}_z - V_g}{D_z^T} dZ'\right). \quad (5)$$

Here D_z^T is the vertical turbulent diffusion coefficient. The ratio of the parameters β for inertial particles β_{in}

and non-inertial particles β_{nonin} is given by

$$\frac{\beta_{\text{in}}}{\beta_{\text{nonin}}} = \alpha \exp\left(-V_g \int_0^Z \frac{dZ'}{D_z^T}\right). \quad (6)$$

Equation (6) allows us to determine the parameter α for inertial particles in the experiments with forced convective turbulence. Here we take into account that for non-inertial particles the parameter $\alpha = 1$. In our experiments the mean fluid velocity as well as the turbulent velocity are much larger than the terminal fall velocity (V_g is about 0.33 cm/s) for inertial particles having the diameter $10\mu\text{m}$.

Using the measured spatial distributions of the normalized mean particle number density $\bar{n}(Y, Z)/\bar{n}_0$ and the mean temperature $\bar{T}(Y, Z)$, we determine the parameter β in every vertical column for inertial particles (having the diameter $10\mu\text{m}$) and non-inertial particles (having the diameter $0.7\mu\text{m}$). All area along the horizontal direction is divided in about 65 vertical columns. We have found that Eq. (4) is valid in our experiments. This procedure yields the dependence of the parameter β on the horizontal coordinate Y . The ratio of these dependencies obtained in the experiments with inertial particles $\beta_{\text{in}}(Y)$ and non-inertial particles $\beta_{\text{nonin}}(Y)$ yields

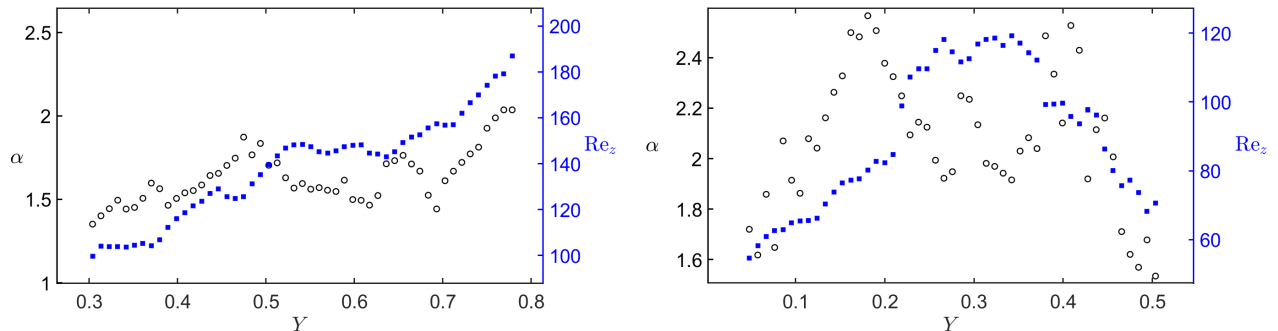


FIG. 14. Dependencies of the parameter α (circles, grey) for inertial particles and the vertical Reynolds number $Re_z = u_z^{\text{rms}} \ell_z / \nu$ (squares, blue) on the horizontal coordinate Y for convective turbulence forced by one oscillating grid (left panel) and by two oscillating grids (right panel). The coordinate Y is normalized by $L_z = 26$ cm.

the dependence of the parameter $\alpha(Y)$ for inertial particles on the horizontal coordinate Y according to Eq. (6). The experiments with inertial and non-inertial particles are performed for the same conditions.

In Fig. 14 we show the dependencies of the parameter α (circles, grey) for inertial particles and the vertical Reynolds number $Re_z = u_z^{\text{rms}} \ell_z / \nu$ (squares, blue) on the horizontal coordinate Y for convective turbulence forced by one oscillating grid (left panel) and by two oscillating grids (right panel). We remind that in the experiments, the vertical gradients of the mean temperature and other fields are much larger than the horizontal gradients, that is why we use the vertical Reynolds number Re_z and the vertical turbulent diffusion coefficient D_z^T . For convective turbulence forced by one oscillating grid, the parameter α for inertial particles increases with the vertical Reynolds number Re_z varying from $\alpha = 1.2$ to $\alpha = 2.4$. For convective turbulence forced by two oscillating grids, the behaviour of the parameter α for inertial particles is more complicated, but it varies from $\alpha = 1.6$ to $\alpha = 2.6$. These results imply that the effect of accumulation of inertial particles is stronger than that for non-inertial particles, which is in an agreement with the theoretical predictions [7, 13].

IV. CONCLUSIONS

Turbulent thermal diffusion of inertial particles characterising a non-diffusive contribution to turbulent flux

of particles, has been studied in laboratory experiments with convective turbulence forced by one or two oscillating grids in the air flow. Fluid velocity field and spatial distribution of inertial particles are measured by Particle Image Velocimetry system, and temperature field is measured using a temperature probe equipped with 12 E - thermocouples. The experiments have shown formation of large-scale clusters of inertial particles in the regions of the mean temperature minimum due to effective pumping velocity directed opposite to the gradient of the mean fluid temperature. As follows from our experiments, the effect of accumulation of inertial particles (having the diameter $10\mu\text{m}$) is stronger than that for non-inertial particles (having the diameter $0.7\mu\text{m}$). In particular, the measured maximum value of the parameter α for inertial particles characterising the large-scale particle clustering reaches $\alpha_{\text{max}} \approx 2.5$, while for non-inertial particles $\alpha = 1$. This implies that the effective pumping velocity causing formation of inertial particle clusters is in 2.5 times larger than that for non-inertial particles. This is in an agreement with the theoretical predictions [7, 13].

AUTHOR DECLARATIONS

Conflict of Interest

The authors have no conflicts to disclose.

DATA AVAILABILITY

The data that support the findings of this study are available from the corresponding author upon reasonable request.

-
- [1] G. T. Csanady, *Turbulent Diffusion in the Environment* (Reidel, Dordrecht, 1980).
 - [2] Ya. B. Zeldovich, A. A. Ruzmaikin, and D. D. Sokoloff, *The Almighty Chance* (Word Scientific Publ., Singapore, 1990).
 - [3] A. K. Blackadar, *Turbulence and Diffusion in the Atmo-*

sphere (Springer, Berlin, 1997).

- [4] J. H. Seinfeld and S. N. Pandis, *Atmospheric Chemistry and Physics. From Air Pollution to Climate Change.*, 2nd ed. (John Wiley & Sons, NY, 2006).
- [5] L. I. Zaichik, V. M. Alipchenkov, and E. G. Sinaiski, *Particles in turbulent flows* (John Wiley & Sons, NY,

- 2008).
- [6] C. T. Crowe, J. D. Schwarzkopf, M. Sommerfeld and Y. Tsuji, *Multiphase flows with droplets and particles*, second edition (CRC Press LLC, NY, 2011).
 - [7] I. Rogachevskii, *Introduction to Turbulent Transport of Particles, Temperature and Magnetic Fields* (Cambridge University Press, Cambridge, 2021).
 - [8] M. Caporaloni, F. Tampieri, F. Trombetti and O. Vittori, Transfer of particles in nonisotropic air turbulence, *J. Atmosph. Sci.* **32**, 565 (1975).
 - [9] M. Reeks, The transport of discrete particle in inhomogeneous turbulence, *J. Aerosol Sci.* **14**, 729 (1983).
 - [10] T. Elperin, N. Kleeorin and I. Rogachevskii, Turbulent thermal diffusion of small inertial particles, *Phys. Rev. Lett.* **76**, 224 (1996).
 - [11] T. Elperin, N. Kleeorin and I. Rogachevskii, Turbulent barodiffusion, turbulent thermal diffusion and large-scale instability in gases, *Phys. Rev. E* **55**, 2713 (1997).
 - [12] A. Guha, A unified Eulerian theory of turbulent deposition to smooth and rough surfaces, *J. Aerosol Sci.* **28**, 1517 (1997).
 - [13] T. Elperin, N. Kleeorin and I. Rogachevskii, Formation of inhomogeneities in two-phase low-Mach-number compressible turbulent fluid flows, *Int. J. Multiphase Flow* **24**, 1163 (1998).
 - [14] A. Guha, Transport and deposition of particles in turbulent and laminar flow, *Annu. Rev. Fluid Mech.* **40**, 311 (2008).
 - [15] Dh. Mitra, N. E. L. Haugen and I. Rogachevskii, Turbophoresis in forced inhomogeneous turbulence, *Europ. Phys. J. Plus* **133**, 35 (2018).
 - [16] F. De Lillo, M. Cencini, S. Musacchio and G. Boffetta, Clustering and turbophoresis in a shear flow without walls. *Phys. Fluids* **28**, 035104 (2016).
 - [17] G. Sardina, P. Schlatter, L. Brandt, F. Picano, and C. M. Casciola, Wall accumulation and spatial localization in particle-laden wall flows. *J. Fluid Mech.* **699**, 50-78 (2012).
 - [18] D. Kaftory, G. Hetsroni, and S. Banerjee, Particle behaviour in the turbulent boundary layer. I. Motion, deposition, and entrainment. *Phys. Fluids* **7**, 1095-1106 (1995).
 - [19] M. Righetti and G. P. Romano, 2004. Particle-fluid interactions in a plane near-wall turbulent flow. *J. Fluid Mech.* **505**, 93 (2004).
 - [20] T. Elperin, N. Kleeorin and I. Rogachevskii, Mechanisms of formation of aerosol and gaseous inhomogeneities in the turbulent atmosphere, *Atmosph. Res.* **53**, 117 (2000).
 - [21] T. Elperin, N. Kleeorin, I. Rogachevskii and D. Sokoloff, Passive scalar transport in a random flow with a finite renewal time: Mean-field equations, *Phys. Rev. E* **61**, 2617 (2000).
 - [22] T. Elperin, N. Kleeorin, I. Rogachevskii and D. Sokoloff, Mean-field theory for a passive scalar advected by a turbulent velocity field with a random renewal time, *Phys. Rev. E* **64**, 026304 (2001).
 - [23] R. V. R. Pandya and F. Mashayek, Turbulent thermal diffusion and barodiffusion of passive scalar and dispersed phase of particles in turbulent flows, *Phys. Rev. Lett.* **88**, 044501 (2002).
 - [24] M. W. Reeks, On model equations for particle dispersion in inhomogeneous turbulence, *Int. J. Multiph. Flow* **31**, 93 (2005).
 - [25] G. Amir, N. Bar, A. Eidelman, T. Elperin, N. Kleeorin and I. Rogachevskii, Turbulent thermal diffusion in strongly stratified turbulence: Theory and experiments, *Phys. Rev. Fluids* **2**, 064605 (2017).
 - [26] N. E. L. Haugen, N. Kleeorin, I. Rogachevskii and A. Brandenburg, Detection of turbulent thermal diffusion of particles in numerical simulations, *Phys. Fluids* **24**, 075106 (2012).
 - [27] I. Rogachevskii, N. Kleeorin and A. Brandenburg, Compressibility in turbulent magnetohydrodynamics and passive scalar transport: mean-field theory, *J. Plasma Phys.* **84**, 735840502 (2018).
 - [28] M. Sofiev, V. Sofieva, T. Elperin, N. Kleeorin, I. Rogachevskii and S. S. Zilitinkevich, Turbulent diffusion and turbulent thermal diffusion of aerosols in stratified atmospheric flows, *J. Geophys. Res.* **114**, D18209 (2009).
 - [29] T. Elperin, N. Kleeorin, Podolak, M., and I. Rogachevskii, A mechanism for the formation of aerosol concentrations in the atmosphere of Titan, *Planetary and Space Science* **45**, 923-929 (1997).
 - [30] A. Hubbard, Turbulent thermal diffusion: a way to concentrate dust in protoplanetary discs, *Monthly Notes Roy. Astron. Soc.* **456**, 3079-3089 (2016).
 - [31] N. Kleeorin and I. Rogachevskii, Large-scale clustering of inertial particles in a rotating, stratified and inhomogeneous turbulence, *Phys. Fluids* **37**, 065152 (2025).
 - [32] J. Buchholz, A. Eidelman, T. Elperin, G. Grünefeld, N. Kleeorin, A. Krein, I. Rogachevskii, Experimental study of turbulent thermal diffusion in oscillating grids turbulence, *Experim. Fluids* **36**, 879 (2004).
 - [33] A. Eidelman, T. Elperin, N. Kleeorin, A. Krein, I. Rogachevskii, J. Buchholz, and G. Grünefeld, Turbulent thermal diffusion of aerosols in geophysics and in laboratory experiments, *Nonl. Proc. Geophys.* **11**, 343 (2004).
 - [34] A. Eidelman, T. Elperin, N. Kleeorin, A. Markovich, I. Rogachevskii, Experimental detection of turbulent thermal diffusion of aerosols in non-isothermal flows, *Nonl. Proc. Geophys.* **13**, 109 (2006).
 - [35] E. Elmakies, O. Shildkrot, N. Kleeorin, A. Levy, I. Rogachevskii, A. Eidelman, Experimental study of turbulent thermal diffusion of particles in inhomogeneous and anisotropic turbulence, *Phys. Fluids* **34**, 055125 (2022).
 - [36] E. Elmakies, O. Shildkrot, N. Kleeorin, A. Levy, I. Rogachevskii, Experimental study of turbulent thermal diffusion of particles in an inhomogeneous forced convective turbulence, *Phys. Fluids* **35**, 095123 (2023).
 - [37] A. Eidelman, T. Elperin, N. Kleeorin, I. Rogachevskii and I. Sapir-Katiraie, Turbulent thermal diffusion in a multi-fan turbulence generator with the imposed mean temperature gradient, *Experim. Fluids* **40**, 744 (2006).
 - [38] E. Zorbib, E. Elmakies, O. Shildkrot, N. Kleeorin, A. Levy, I. Rogachevskii, Experimental investigation of turbulence and turbulent thermal diffusion in strongly inhomogeneous and anisotropic forced convection, *Phys. Fluids* **37**, 115145 (2025).
 - [39] I. Shimberg, O. Shriki, O. Shildkrot, N. Kleeorin, A. Levy, I. Rogachevskii, Experimental study of turbulent transport of nanoparticles in convective turbulence, *Phys. Fluids* **34**, 055126 (2022).
 - [40] R. J. Adrian, Particle-imaging techniques for experimental fluid mechanics, *Annu. Rev. Fluid Mech.* **23**, 261 (1991).
 - [41] M. Raffel, C. Willert, S. Werely and J. Kompenhans, *Particle Image Velocimetry* (Springer, Berlin-Heidelberg, 2007).
 - [42] J. Westerweel, Theoretical analysis of the measurement

- precision in particle image velocimetry, *Experim. Fluids* **29**, S3 (2000).
- [43] P. Guibert, M. Durget and M. Murat, Concentration fields in a confined two-gas mixture and engine in cylinder flow: laser tomography measurements by Mie scattering, *Experim. Fluids* **31**, 630-642 (2001).
- [44] C. F. Bohren and D. R. Huffman, *Absorption and Scattering of Light by Small Particles* (John Wiley and Sons, New York, 1983).
- [45] M. Bukai, A. Eidelman, T. Elperin, N. Kleeorin, I. Rogachevskii and I. Sapir-Katiraie, Transition phenomena in unstably stratified turbulent flows, *Phys. Rev. E* **83**, 036302 (2011).
- [46] M. Bukai, A. Eidelman, T. Elperin, N. Kleeorin, I. Rogachevskii and I. Sapir-Katiraie, Effect of large-scale coherent structures on turbulent convection, *Phys. Rev. E* **79**, 066302 (2009).
- [47] L. Barel, A. Eidelman, T. Elperin, G. Fleurov, N. Kleeorin, A. Levy, I. Rogachevskii, O. Shildkrot, Detection of standing internal gravity waves in experiments with convection over a wavy heated wall, *Phys. Fluids* **32**, 095105 (2020).
- [48] A. Eidelman, T. Elperin, I. Gluzman, N. Kleeorin, I. Rogachevskii, Experimental study of temperature fluctuations in forced stably stratified turbulent flows, *Phys. Fluids* **25**, 015111 (2013).
- [49] N. Cohen, A. Eidelman, T. Elperin, N. Kleeorin, I. Rogachevskii, Sheared stably stratified turbulence and large-scale waves in a lid driven cavity, *Phys. Fluids* **26**, 105106 (2014).
- [50] A. Eidelman, T. Elperin, N. Kleeorin, G. Hazak, I. Rogachevskii, O. Sadot, I. Sapir-Katiraie, Mixing at external boundary of submerged turbulent jet, *Phys. Rev. E* **79**, 026311 (2009).
- [51] A. Eidelman, T. Elperin, N. Kleeorin, B. Melnik and I. Rogachevskii, Tangling clustering of inertial particles in stably stratified turbulence, *Phys. Rev. E* **81**, 056313 (2010).
- [52] J. S. Turner, The influence of molecular diffusivity on turbulent entrainment across a density interface, *J. Fluid Mech.* **33**, 639-656 (1968).
- [53] S. T. Turner, *Buoyancy Effects in Fluids* (Cambridge Univ. Press, Cambridge, 1973).
- [54] S. M. Thompson and J. S. Turner, Mixing across an interface due to turbulence generated by an oscillating grid, *J. Fluid Mech.* **67**, 349-368 (1975).
- [55] E. J. Hopfinger and J.-A. Toly, Spatially decaying turbulence and its relation to mixing across density interfaces, *J. Fluid Mech.* **78**, 155-175 (1976).
- [56] E. Kit, E. J. Strang and H. J. S. Fernando, Measurement of turbulence near shear-free density interfaces, *J. Fluid Mech.* **334**, 293-314 (1997).
- [57] M. A. Sánchez and J. M. Redondo, Observations from grid stirred turbulence, *Appl. Sci. Res.* **59**, 243-254 (1998).
- [58] P. Medina, M. A. Sánchez and J. M. Redondo, Grid stirred turbulence: applications to the initiation of sediment motion and lift-off studies, *Phys. Chem. Earth* **B 26**, 299-304 (2001).